Bitstream Photon Counting Chirped AM Lidar with a Dual Unipolar Signal

Brian C. Redman, retired - no institutional affiliation, email: bredman@rocketmail.com

Abstract

This paper is a follow-up to three previous papers: the first introducing the new Bitstream Photon Counting Chirped Amplitude Modulation (AM) Lidar (PC-CAML) with the unipolar Digital Logic Local Oscillator (DLLO) concept, the second introducing the improvement thereof using the bipolar DLLO, and the third introducing the improvement of digital In-phase and Quadrature-phase (I/Q) demodulation.

In that previous work, the signal was a single unipolar chirped sinusoidal or square wave. This paper introduces a new bitstream PC-CAML transceiver architecture that combines two unipolar chirped signals, referred to as the dual unipolar signal, to form a single bipolar signal in the receiver. (patent pending) This bipolar signal is mixed with the bipolar DLLOs in the in-phase (I) digital mixing and quadrature-phase (Q) digital mixing channels for digital I/Q demodulation for improved signal-to-noise ratio (SNR) compared to that when using a single unipolar signal.

The simulation results presented in this paper indicate an SNR improvement for the dual unipolar chirped sinusoidal signal bitstream PC-CAML compared to that of the unipolar chirped sinusoidal signal bitstream PC-CAML (both with bipolar DLLOs and digital I/Q demodulation) of from about 3 dB to about 6 dB for signals below the onset of receiver saturation, and an improvement for maximum achievable SNR of about 13 dB if the receiver is allowed to saturate.

The bitstream PC-CAML with a dual unipolar signal and bipolar DLLOs with digital I/Q demodulation architecture discussed in this paper adds complexity to the transmitter and receiver compared to the architectures presented in the previous papers. Whether or not this additional complexity is worth the improved SNR will have to be decided as part of system trade studies for particular systems and their applications.

However, the new architecure still retains the key advantages of the previous bitstream PC-CAML architectures since it still replaces bulky, power-hungry, and expensive wideband RF analog electronics in the receiver with digital components that can be implemented in inexpensive silicon complementary metal-oxide-semiconductor (CMOS) read-out integrated circuits (ROICs) to make the bitstream PC-CAML with a DLLO more suitable for compact lidar-on-a-chip systems and lidar array receivers than previous standard PC-CAML systems.

This paper introduces the dual unipolar signal and bipolar DLLOs with digital I/Q demodulation transceiver architecture for bitstream PC-CAML, and presents the initial SNR theory with comparisons to Monte Carlo simulation results.

1. Dual Unipolar Signal for Bitstream PC-CAML Concept

The standard patented photon counting chirped amplitude modulation lidar (PC-CAML) concept has been extensively discussed previously. [ref 1-14] In previous standard PC-CAML systems, the local oscillator (LO) has been a radio-frequency (RF) analog signal applied using expensive, bulky, and power hungry RF analog electronics either in post-detection mixing or via opto-electronic mixing (OEM) at the photon counting detector, including gating of the detector, or applied via pre-detection mixing using an optical intensity modulator. Also in previous PC-CAML systems, the signal has been a single unipolar chirped waveform. The reader is referred to references 1-14 for more details on the theory and practice for the standard PC-CAML system.

This paper is a follow-up to three previous papers: the first introducing the new Bitstream Photon Counting Chirped Amplitude Modulation (AM) Lidar (PC-CAML) with the unipolar Digital Logic Local Oscillator (DLLO) concept [ref 15], the second introducing the improvement thereof using the bipolar DLLO [ref 16], and the third introducing the improvement of digital In-phase and Quadrature-phase (I/Q) demodulation [ref 17]. Reading the previous papers [ref 15-17] before proceeding to read this paper is recommended.

In the previous work, the signal was a single unipolar chirped sinusoid or square wave. This paper introduces a new bitstream PC-CAML transceiver architecture that combines two unipolar chirped signals, referred to as the dual unipolar signal, to form a single bipolar signal in the receiver. (patent pending [ref 18]) This bipolar signal is mixed with the bipolar DLLOs in the in-phase (I) and quadrature-phase (Q) digital mixing channels for digital I/Q demodulation for improved signal-to-noise ratio (SNR) compared to that provided by a single unipolar signal.

The simulation results presented in section 3, figure 2, of this paper indicate an SNR improvement for the dual unipolar chirped sinusoidal signal bitstream PC-CAML compared to that of the unipolar chirped sinusoidal signal bitstream PC-CAML [ref 17] (both with bipolar DLLOs and digital I/Q demodulation) of from about 3 dB to about 6 dB for signals below the onset of receiver saturation, and an improvement for maximum achievable SNR of about 13 dB if the receiver is allowed to saturate.

The bitstream PC-CAML with a dual unipolar signal and bipolar DLLOs with digital I/Q demodulation architecture discussed in this paper adds complexity to the transmitter and receiver compared to the architectures presented in the previous papers. Whether or not this additional complexity is worth the improved SNR will have to be decided as part of system trade studies for particular systems and their applications.

However, the new architecure still retains the key advantages of the previous bitstream PC-CAML architectures [ref 15-17] since it still replaces bulky, power-hungry, and expensive wideband RF analog electronics in the receiver with digital components that can be implemented in inexpensive silicon complementary metal-oxide-semiconductor (CMOS) read-out integrated circuits (ROICs) to make the bitstream PC-CAML with a DLLO more suitable for compact lidar-on-a-chip systems and lidar array receivers than previous PC-CAML systems.

This paper introduces the dual unipolar signal and bipolar DLLOs with digital I/Q demodulation transceiver architecture for bitstream PC-CAML, and presents the initial SNR theory with comparisons to Monte Carlo simulation results.

It is well known that since there cannot be negative optical power or intensity, the chirped AM (aka intensity modulation (IM)) optical signal is naturally unipolar. It is also well known that the unipolar chirped AM signal has an electrical power SNR that is a factor of 4 (6 dB) lower than that of an equivalent bipolar signal due to a 3 dB loss of signal power to the DC component and a 3 dB lower peak power as discussed in references 2-4.

In order to recover the SNR losses due to the unipolar nature of the chirped AM optical signal, the new dual unipolar signal technique was invented by the author and is presented herein. (patent pending [ref 18]) In this new technique, there are two optical signal channels, either split from one source prior to modulation, or from two different modulated sources. The modulation for channel 1 consists of the positive amplitude portions of a bipolar chirped sinusoid or square wave, between which there are zeros (no signal) where the negative amplitude portion of the bipolar chirped waveform was. The modulation for channel 2 consists of the negative amplitude portions of the same bipolar chirped sinusoid or square wave, between which there are zeros (no signal) where the positive amplitude portion of the bipolar chirped waveform was, but inverted in polarity to be a positive unipolar signal.

Each optical signal channel must be tagged uniquely so that they can be separated cleanly from each other in the receiver after having been combined into a single transmitted beam. This tagging can be done by each channel having a different optical carrier frequency/wavelength from each other, having orthogonal polarizations with respect to each other, or having uncorrelated or orthogonal modulation codes applied to them (as is done in optical code division multiple access (CDMA) communications), for example.

Using orthogonal polarizations for tagging the two channels is problematic for lidar since the target and/or the propagation medium may be depolarizing.

The use of CDMA modulation for tagging the two channels has the advantage of requiring only a single wavelength source in the transmitter and a single detector in the receiver for the two channels, but is complicated by decoding synchronization issues due to different delay times between transmission and reception for multiple targets at different ranges.

If one uses a code with a short enough chip duration to separate the targets at different ranges using a bank of code filters with different delays, then one may as well dispense with using the chirped AM modulation and use the code modulation for ranging.

Instead, one may be able to use a long code chip duration that is longer than the unambiguous range interval of interest so that all of the targets' delays are within a single chip duration and the received code is synchronized within a single chip duration for all targets of interest. In this case, synchronous CDMA with orthogonal codes might be possible. However, the duration of the chirp would need to be the number of chips in the code times longer than the chip duration, which may be quite long if the unambiguous range and/or the number of chips in the code are large. In addition, for code tagging, On-Off-Keying (OOK) is not recommended since this would reduce the transmitted power in the signal. Instead, binary phase shift keying (BPSK) of the chirped AM signal's phase would be preferred since all of the transmitted signal power would be utilized in that case. Because of these issues and complexities, the use of CDMA tagging is beyond the scope of this introductory paper, and is suggested for investigation in future work.

Therefore, for clarity, the channel tagging for the dual unipolar signal discussed in this introductory paper is optical carrier frequency/wavelength tagging (aka wavelength tagging).

The optical carriers at two different wavelengths can be generated from two different sources, or from a single source followed by a frequency/wavelength shifter such as an acousto-optic modulator (AOM), electro-optic modulator (EOM), frequency doubler, Raman amplifier, or parametric amplifier, for example. The requirement on the wavelength difference between the two channels is that it is large enough that the two channels' optical spectra do not overlap. It is not necessary that the two wavelengths be in the same optical waveband since different detector types with different spectral responses may be employed in the receiver. However, it may be simpler to use the same type of detector for each channel, in which case, the two wavelengths should be in the same spectral response waveband as the detector.

The use of a low cost, directly current modulated, low power, continuous wave (cw) semiconductor laser as the optical source for each wavelength channel is an attractive option. The optical linewidth of each laser needs to be narrow enough to minimize losses in the receiver's narrow band optical filters, but a temporally coherent single-frequency laser is not required. The wavelength separation between the two sources also needs to fit within the gain bandwidth of the optional optical amplifier used to increase the transmitted optical power, if needed, after the two channels are combined into a single beam for transmission.

On the order of one to a few nanometer filter linewidths are typically used with photon counting detectors in the presence of daytime solar backgrounds. The laser linewidths would need to be about half of the filter linewidth or less to insure good transmission through such filters in the presence of manufacturing tolerances on both the laser and filter center wavelengths and linewidths, and to provide margin for optical Doppler frequency shifts for fast moving targets.

The difference between the two wavelengths should be at least a few times the filter linewidth to minimize spectral overlap so the two wavelengths can be cleanly separated in the receiver.

A representative set of parameters might be on the order of 0.5 nm laser linewidth, 1 nm filter linewidth, and 8 nm wavelength separation between the center wavelengths. The total bandwidth of less than 10 nm for the two sources in this case is well within the typical gain bandwidths of tens of nanometers for semiconductor and fiber optical amplifiers. A dichroic beamsplitter with no more than 7 nm edge steepness to combine/separate the two wavelengths is within the current capabilities of commercially available multilayer interference filters. Even smaller wavelength separations could be used with gratings or holographic filters for bulk optics, or other wavelength division multiplexing (WDM) de-multiplexing (demux) technologies in waveguides.

Figure 1 shows block diagrams for the transceiver architecture for the bitstream PC-CAML with a dual unipolar signal and bipolar DLLOs with digital I/Q demodulation using wavelength tagging. Figure 1 (a.) shows the transmitter architecture block diagram, and 1 (b.) shows the receiver architecture block diagram. The modulation waveforms are also illustrated in figure 1.

In figure 1 (a.) a digital chirped signal generator outputs the same, synchronized digital bipolar chirped sinusoidal or square wave signal on two channels. Digital signal processing circuitry in channel 1/2 retains the positive/negative amplitude portion of the bipolar chirped signal and replaces the negative/positive amplitude portion with zeros, respectively. Digital signal processing circuitry in channel 2 then inverts the polarity of the waveform.

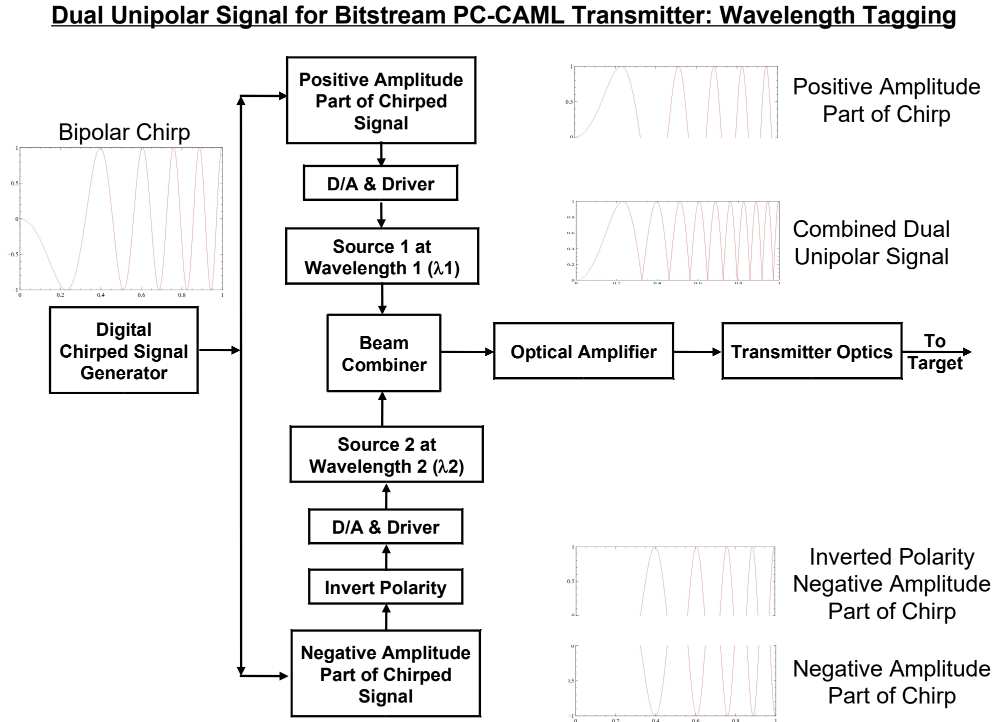

(a.)

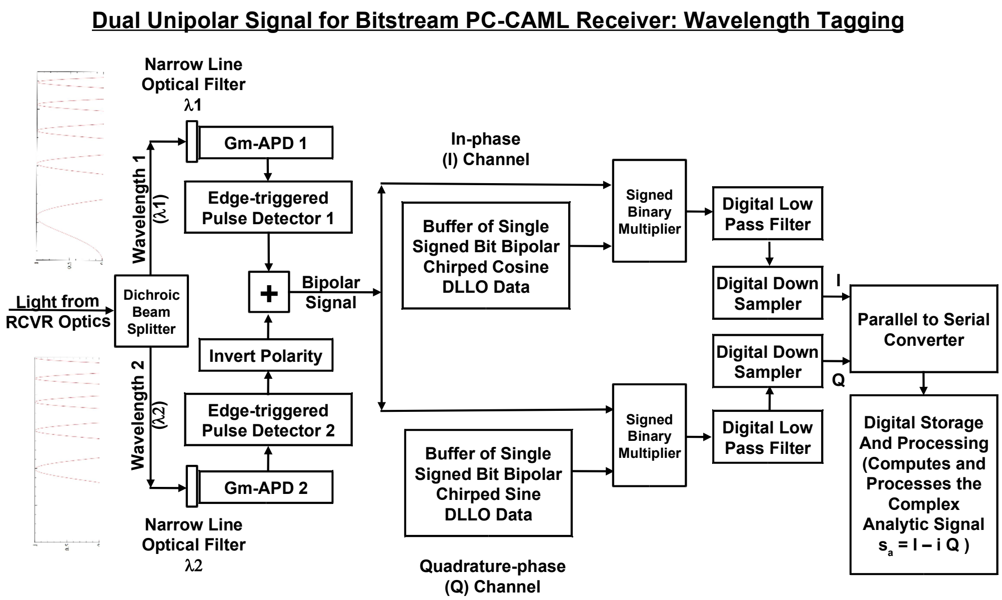

(b.)

Figure 1. Bitstream PC-CAML with a Dual Unipolar Signal using wavelength tagging transceiver architecture block diagram (a.) transmitter architecture block diagram and (b.) receiver architecture block diagram.

A digital-to-analog (D/A) converter and analog driver circuitry in each channel converts the resulting unipolar waveform for each channel into a drive current that modulates the output power of the low power continuous wave (cw) semiconductor laser source in that channel. The laser in channel 1 operates at wavelength 1 ($\lambda 1$), and the laser in channel 2 operates at wavelength 2 ($\lambda 2$). An optical beam combiner combines the laser outputs at the two wavelengths into a single beam. Note that the difference in path delays between the two channels needs to be less than a small fraction of the smallest period in the chirp waveform to maintain synchrony between the waveforms in the two channels.

The single two-wavelength beam with the combined channels 1 and 2 waveforms is amplified by an optical amplifier and transmitted through transmitter beam shaping optics to the targets.

Note that the optics in the transmitter system may be fiber optical components, waveguide components, and/or bulk optical components.

In figure 1 (b.), the light from the receiver optical system is split by a wavelength splitting device, such as a dichroic beam splitter, into two separate wavelength channels, one centered at wavelength 1 of transmitter channel 1 and the other centered at wavelength 2 of transmitter channel 2. The received light in each channel is transmitted through a narrow line optical filter centered at the center wavelength of that channel.

Note that the optics in the receiver system may be fiber optical components, waveguide components, and/or bulk optical components.

The filtered received light in each channel is detected by a Geiger-mode Avalanche Photodiode Detector (Gm-APD) (also known as a single-photon avalanche diode (SPAD)) photon counting detector. In each channel, the constant amplitude output count of the Gm-APD is input to an edge-triggered pulse detector which outputs a shorter single bit binary digital logic level pulse. The output of the edge-triggered pulse detector in channel 2 is inverted in polarity, and then added to the output of the edge-triggered pulse detector of channel 1, resulting in the bipolar received signal plus noise signed binary digital data.

This bipolar signal plus noise signed binary digital data is duplicated so that one copy is routed to the in-phase (I) channel and the other copy is routed to the quadrature-phase (Q) channel. The bipolar signal plus noise signed binary digital data in each I/Q channel is multiplied by the bipolar digital logic local oscillator (DLLO) signed binary digital data of the corresponding channel. This signed binary multiplication may be implemented using a bipolar Boolean exclusive OR (XOR) or exclusive NOR (XNOR) binary digital logic gate, or using any other signed binary digital processing method. The bipolar DLLO data in each channel can be generated and stored in a data buffer prior to operation of the lidar. The DLLO data buffers may be circular buffers to enable continuous repetition of the waveform.

The signed binary digital data output from each multiplier are then sent to a corresponding digital low pass filter, the output of which is sent to a corresponding digital down sampler. The in-phase (I) and the quadrature-phase (Q) signals from the digital down samplers are input to a parallel to serial converter which outputs the I and Q signals digital data on a single serial line to the inputs of the digital data storage and processing subsystem. The digital signal processor (DSP) in this subsystem combines the real-valued I and Q data into the complex analytic signal data, $s_a = I–iQ$, where $i=(-1)^{½}$, and computes the power spectrum of s_a given by $S_a = |cfft(s_a)|^2$, where cfft(argument) is the complex fast Fourier transform (FFT) of the argument, and |expression| is the magnitude of the enclosed expression.

The DSP finds peaks in the power spectrum S_a, which represent target returns. The frequency of a peak in S_a is proportional to a target range just as in the standard data processing for the standard PC-CAML.

The edge-triggered pulse detector allows the single-bit signal pulses to be much shorter than the count pulses output by the Gm-APD, which may be longer than desired due to the dead-time. The edge-triggered pulse detector's output pulse can be as short as a single clock pulse.

1.1 Key Advantages of the Dual Unipolar Signal for Bitstream PC-CAML

The key advantages of the dual unipolar signal with bipolar DLLOs and digital I/Q demodulation in the bitstream PC-CAML are as follows:

1. The receiver architecture can be implemented in the unit cells of a photon counting receiver's readout integrated circuit (ROIC) by adding the signed binary digital circuitry indicated in the receiver architecture.
2. The bipolar signal plus noise data and the in-phase and quadrature-phase DLLO data each consist of just a stream of signed binary digital data.
3. The signed binary digital circuitry eliminates the need for bulky, power-hungry, and expensive wideband RF analog electronics by replacing them with digital electronics. Multi-GHz clocks and digital circuits are readily implemented in inexpensive silicon complementary metal-oxide-semiconductor (CMOS) ROICs.
4. The in-phase and quadrature-phase bipolar DLLO signed binary data can be computed prior to operation and stored in buffers in each ROIC unit cell, or in a single buffer for each of the in-phase and quadrature-phase bipolar DLLOs in the receiver and distributed to each ROIC unit cell in real-time during operation. The buffers may be circular buffers for continuous repetition of the in-phase and quadrature-phase bipolar DLLO waveforms.
5. The dual unipolar signal improves the electrical power SNR by from about 3 dB to about 6 dB compared to that of the unipolar signal, with both using bipolar DLLOs and digital I/Q demodulation, for signals below the onset of receiver saturation, and provides an improvement for maximum achievable SNR of about 13 dB if the receiver is allowed to saturate.

The bitstream PC-CAML with a dual unipolar signal and bipolar DLLO with digital I/Q demodulation architecture discussed in this paper adds complexity to the transmitter and receiver compared to the architectures presented in the previous papers [ref 15-17]. With wavelength tagging of the two channels, two sources, or one source and a wavelength shifter are required in the transmitter. Two optical filters, two Gm-APDs, and two edge-triggered pulse detectors are required in the receiver. (The use of CDMA code tagging would require only one source in the transmitter, and one optical filter, one Gm-APD, and one edge-triggered pulse detector in the receiver, but it has other complexities that require investigation in future work.) Whether or not the additional complexity, which may translate to increased size, weight, power, and cost compared to the previous bitstream PC-CAML architectures [ref 15-17], is worth the improved SNR will have to be decided by system trade studies for particular systems and applications.

2. Bitstream PC-CAML with a Dual Unipolar Signal SNR Theory

The purpose of this paper is to introduce the new dual unipolar signal technique for bitstream PC-CAML, and to show through simulation results how it works. The purpose of this paper is not to develop a comprehensive theory of operation for the new technique, so the initial SNR theory presented herein has a limited range of applicability to the new technique, and an improved theory needs to be developed in future work.

The initial electrical power signal-to-noise ratio (SNR) theory used herein for the bitstream PC-CAML with the dual unipolar signal and bipolar DLLOs with digital I/Q demodulation technique is derived from the SNR theory for photon counting Gm-APDs developed by Gatt, Johnson, and Nichols. [ref 19, pp. 3268-3269] and its modification for bitstream PC-CAML with the unipolar signal and bipolar DLLOs with digital I/Q demodulation as described in reference 17. The theory developed by Gatt, et. al., is for detection of unmodulated pulsed lidar returns. This theory, however, can be applied to the dual unipolar signal with bipolar DLLOs and digital I/Q demodulation as simulated in Mathcad®[1] by making the following adjustments:

1. Adding quantization noise due to the quantization for signed binary bipolar signals, DLLOs, and intermediate frequency (IF) signals.
2. Setting the arm probability, PA, in the SNR equations of Gatt, et. al., [ref 19, pp. 3268-3269] to 1 since in the theory as used herein, the counts per matched filter impulse response time are output counts after having been subjected to the arm probability.
3. Multiplying the theoretical SNR by $10^{-0.176}$ to account for the scalloping loss due to the Hann window applied to the data in the simulations (see section 3) to reduce sidelobes.

Equation (41) from Gatt, et. al., [ref 19, p. 3269] modified as described above becomes

$$SNR_{theory} = \frac{10^{-0.176} N_s \left[1-\left(\frac{M}{M+m_{scounts}}\right)^M\right]^2}{\left[1-e^{-\left(m_{ncounts}+m_{qncounts}\right)}\left(\frac{M}{M+m_{scounts}}\right)^M\right]\left[1-\left[1-e^{-\left(m_{ncounts}+m_{qncounts}\right)}\cdot\left(\frac{M}{M+m_{scounts}}\right)^M\right]\right]} \qquad (1.)$$

where N_s = Number of clock time interval samples accumulated over the chirp duration
M = speckle diversity
$m_{scounts}$ = average number of signal counts output by the Gm-APD per clock time interval
$m_{ncounts}$ = average number of noise counts output by the Gm-APD per clock time interval (includes all of the additive noise sources except for quantization noise)
$m_{qncounts}$ = the average number of quantization noise counts per clock time interval.

Note that the clock time interval equals the matched filter impulse response time and the dead-time in this theory and in the simulations discussed in section 3.

This SNR theory does not include the effects of energy losses to higher order harmonics and their mixing products. This SNR theory also assumes 100% modulation depth for the signal.

1 Mathcad® is a registered trademark of PTC Inc. or its subsidiaries in the U.S. and in other countries.

2.1 No Modulation Depth Loss Near Saturation for the Dual Unipolar Chirped Sinusoid

As the average number of signal counts output by the Gm-APD per available clock time interval increases towards 1, the apparent modulation depth of the unipolar sinusoidal chirped AM waveform decreases due to the Gm-APD being able to output at most only a single count per dead-time. For the unipolar sinusoidal signal, when the average count rate is so high that a count is output for every clock time interval, the single-bit count data stream looks like that of a constant, unmodulated signal corresponding to a modulation depth of zero and therefore, the SNR goes to zero. This effect was evident in the SNR results graphs for the unipolar chirped sinusoidal waveform presented in the previous papers. [ref 15-17]

For the fully modulated dual unipolar signal in each channel, however, the clock time interval samples where there are zero's in a channel's waveform are never filled by 1's for any signal level, and those clock time interval samples can only have an occasional 1 due to noise at the low noise levels in the simulations and in a well designed PC-CAML. Thus, as $m_{s\_counts\_avg}$ approaches 1, only the clock time interval samples corresponding to the non-zero levels of the dual unipolar signal in each channel become filled with 1's, causing the waveform in each channel to approach the uniformly sampled deterministic unipolar chirped square wave as $m_{s\_counts\_avg}$ approaches 1.

2.2 Different Effects of Speckle Diversity on Unipolar and Dual Unipolar Sinusoidal Signals

As shown by the Monte Carlo simulation results in references 15-17, the value of the speckle diversity, M, affects the SNR for the unipolar chirped sinusoidal signal as predicted by the SNR theory. However, the Monte Carlo simulation results in section 3, figure 2 of this paper show that the value of M makes no significant difference in the SNR for the fully modulated dual unipolar chirped sinusoidal signal in contrast to the theory's predictions. This was also the case for the fully modulated unipolar chirped square wave signal as shown by the Monte Carlo simulation results in section 3, figure 6 (b.) of ref 15. The following is an untested conjecture to explain these results, but more work on the SNR theory is clearly needed.

For each channel of the fully modulated dual unipolar chirped sinusoidal signal, and for the fully modulated unipolar chirped square wave, where the signal is zero, there are no speckle induced signal fluctuations since there are no signal counts in those areas, just noise counts. Although the photon arrival rates will vary with the speckle amplitude fluctuations in the non-zero areas of the signal, this may just look like additive random sampling of the those areas of the signal with a different distribution of random samples depending on M, which does not change the SNR. Therefore, for the fully modulated dual unipolar chirped sinusoidal signal, this causes the effect of the speckle induced signal amplitude fluctuations on the SNR to be nearly eliminated for the same reason that it was also eliminated in the results for the fully modulated unipolar chirped square wave signal presented in reference 15.

For the fully modulated unipolar chirped sinusoidal signal there is some signal everywhere except at the exact nulls of the waveform so that the speckle induced amplitude fluctuations cause photon arrival rate fluctuations at almost all points on the signal, and these fluctuations are higher for lower M causing the SNR to be lower for lower M just as seen in the Monte Carlo simulation results and theory predictions for the unipolar chirped sinusoidal signal. [ref 15-17]

For the sake of brevity, this paper discusses only the dual unipolar chirped sinusoidal signal, whereas reference 15 discussed both the unipolar chirped sinusoidal signal and the unipolar chirped square wave signal. However, the dual unipolar signal may be either a chirped sinusoidal signal or a chirped square wave signal.

2.3 Quantization Noise for the Dual Unipolar Signal with the Bipolar DLLO

Noise due to quantization must be calculated to use in the SNR theory of equation (1.). The quantization noise is computed from the Signal-to-Quantization-Noise Ratio in dB ($SQNR_{dB}$) given by equation 2.38 of Bjorndal [ref. 20, p. 40]:

$$SQNR_{dB} = 6.02 * N_{bits} + 1.76, \text{ where } N_{bits} = \text{the number of bits of digitization.} \quad (2.)$$

The number of bits input to equation (2.) for the dual unipolar signal with a bipolar DLLO technique is determined as follows.

For the Bipolar DLLO multiplied by the Bipolar Signal resulting from processing the Dual Unipolar Signal in the receiver, there are 3 states (+1, 0, -1) since +0 and -0 are equivalent, degenerate states equal to 0. Therefore, the equivalent number of bits is derived from

$$2^{N_{bits}} = 3 \Longrightarrow N_{bits} \cdot \ln(2) = \ln(3) \Longrightarrow N_{bits} = \ln(3)/\ln(2) = 1.5849625 \quad (3.)$$

Therefore, $SQNR\_dB(N_{bits}=1.5849625) = 6.02*1.5849625 + 1.76 = 11.301474$ dB, and $SQNR = 10^{1.1301474} = 13.4942$.

Thus, the quantization noise per count is 1/13.4942 for N_{bits}=1.5849625 corresponding to 3 states.

The above calculation applies to the N_{bits} quantization noise for the IF data using the unipolar signal and unipolar DLLO with the AND logic gate digital mixer as described in reference 15. However, Klein states and shows that "…the logic function XOR results in the negative multiplication of two bipolar bit-streams, and the logic function AND results in the multiplication of two unipolar bit-streams...For the logic operation XOR, the standard deviation is doubled in comparison to the operations OR and AND...Due to the fact that the output bit stream changes from zero to one with XOR and only from 0.5 to zero or one with OR and AND, the scaling is expected to be a factor of two of the standard deviations from OR and AND to XOR." [ref 21]

Since for the electrical power SNR, the noise is given by the variance rather than the standard deviation, the quantization noise for the bipolar signal multiplied by the bipolar DLLO is 4 times higher than that for the unipolar signal multiplied by the unipolar DLLO with the same number of quantization bits. Therefore, for the bipolar signal and bipolar DLLO, the average number of quantization noise counts per clock time interval is given by:

$$m_{q\_n\_counts\_avg} = 4 \cdot m_{spn\_counts\_avg}/13.4942 = m_{spn\_counts\_avg}/3.37355 \quad (4.)$$

where $m_{q\_n\_counts\_avg}$ = the average number of quantization noise counts per clock time interval in the simulations

$m_{spn\_counts\_avg}$ = the average number of signal plus noise counts per clock time interval in the simulations.

Therefore, the average number of quantization noise counts per clock time interval for the bipolar signal and bipolar DLLO is 1.78 times higher than that of the unipolar signal and unipolar DLLO, which is given by $m_{spn\_counts\_avg}/6$. [ref 15]

In the initial SNR theory, equation (1.), $m_{qncounts}$ is set equal to the value of $m_{q\_n\_counts\_avg}$ from equation (4.) for comparison to the simulation results.

Development of an SNR theory that includes the effects of quantization noise, aliasing, the harmonics and their mixing products, any signal modulation depth, synchronization errors between the dual unipolar signal channels, and Gm-APD saturation for the bitstream PC-CAML that is applicable for unipolar and dual unipolar chirped sinusoidal and square wave signals is beyond the scope of this paper and is suggested for future work.

3. Monte Carlo Simulation Results Compared to Initial SNR Theory

The equations and functions for implementing the Monte Carlo simulations of signal and noise for bitstream PC-CAML with the unipolar signals and the unipolar and bipolar DLLOs with a single digital mixing channel and with I/Q demodulation in Mathcad® were given in the previous papers. [ref 15-17]

The only changes for the dual unipolar signal with bipolar DLLOs and digital I/Q demodulation simulations are as follows:

1. Using the dual unipolar signal equations shown in equations (5 b.) and (5 c.) below, derived from the bipolar chirped sinusoidal signal shown in equation (5 a.) below.
2. Using zero padding to 4 times the original signal length instead of 8 times the original signal length as used in the previous papers since 8 times zero padding caused memory problems in generating and processing two unipolar signals in the dual unipolar signal case that had not occurred for the one unipolar signal used in the previous work. [ref 15-17] Note that the 4 times zero padding was sufficient to provide good results.

The equations for the bipolar chirped sinusoidal signal and the two unipolar chirped sinusoidal signals derived from it are given by

$$\text{signal} := \overrightarrow{\sin\left[2\cdot\pi\cdot\left[f_0 + k_f\cdot\left(t - \frac{2\cdot R_{tgt}}{c} - \tau_{txdelay}\right)\right]\cdot t\right]} \qquad (5\ \text{a.})$$

$$\text{signal1}_i := \text{if}(\text{signal}_i > 0, \text{signal}_i, 0) \qquad (5\ \text{b.})$$

$$\text{signal2}_i := \text{if}(\text{signal}_i < 0, -\text{signal}_i, 0) \qquad (5\ \text{c.})$$

where f_0 = the start frequency of the chirp
k_f = the temporal slope of the chirp = $(f_s - f_0)/T_{chirp}$, where f_s = the stop frequency

of the chirp, and T_{chirp} = the duration of the chirp
t = the clock time from the start of the chirp
i = index over clock time intervals
if(*arg1, arg2, arg3*) = *arg2* if *arg1* is true; *arg3*, otherwise.

In the simulations, the mean number of signal photoelectrons in a clock time interval prior to applying the dead-time and arm probability restrictions on the detected counts is modulated by each of the signals resulting from equations (5 b.) and (5 c.) for input to the negative binomial random number generator for each channel of the dual unipolar signal in the same way as for the single unipolar signal as detailed in reference 15.

Each of the unipolar signals' random realizations are then subjected to the restriction of the Gm-APD's output having at most a single signal plus noise count per dead-time which is set equal to the clock time interval in the simulations, in the same way as detailed for the single unipolar signal in reference 15. The resulting single-bit unipolar random signal plus noise count data stream for each channel is then processed and combined into a single bipolar random signal plus noise signed binary digital data stream as indicated in figure 1 (b.).

The bipolar signal plus noise binary digital data stream is duplicated with one copy being multiplied by the bipolar chirped cosine DLLO signed binary digital data for the in-phase (I) channel, and the other copy being multiplied by the bipolar chirped sine DLLO signed binary digital data for the quadrature-phase (Q) channel to form the digitally mixed I and Q intermediate frequency (IF) signals plus noise in accordance with figure 1 (b.). The I and Q IF signals are combined as follows to form the complex analytic signal:

$$IQ\_cplx = Mixed\_I - i\, Mixed\_Q \qquad (6.)$$

where Mixed_I = the I bipolar DLLO times the bipolar signal plus noise data
Mixed_Q = the Q bipolar DLLO times the bipolar signal plus noise data
$i = (-1)^{1/2}$

The complex analytic signal is Hann windowed to reduce sidelobes in the IF power spectrum. The Hann windowed complex analytic signal is zero padded to four times the original length.

The power spectrum of the Hann windowed and zero padded complex analytic signal is computed in Mathcad® for each trial. The resulting power spectra are averaged together to produce the mean power spectrum for all the trials.

The mean noise floor of this mean power spectrum is computed over the portion of the spectrum between the target signal's fundamental IF and the fifth harmonic of that frequency since this is the first higher harmonic visible in the IF spectrum of the dual unipolar signal as it squares off at higher signal levels due to Gm-APD saturation. The value of this mean noise floor is the denominator in computing a simulation's mean SNR.

The peak value of the mean power spectrum at the fundamental IF minus the value of the mean noise floor is used as the numerator in computing a simulation's mean SNR.

Note that since the simulated data are quantized, the quantization noise is inherently included in the simulated power spectra.

The Monte Carlo simulations generate 24 realizations of signal plus noise for an up-chirp AM signal waveform. The simulations were run for the following parameter values:

N_{trials} = Number of simulation trials = 24	N_s = Number of clock time intervals = 2^{13}
Δt = Clock time interval = 0.5 ns	t_{chirp} = chirp duration = 4.096 µs
f_0 = 100 MHz = chirp start frequency	f_s = 500 MHz = chirp stop frequency
Target Range = 2.99963379 m	Target IF = 1.953125 MHz
M = speckle diversity = 1 or 1E+06	

$m_{n\_counts\_avg}$ = average number of additive noise counts per clock time interval = 2E-04
$m_{s\_counts\_avg}$ = average number of signal counts per clock time interval = from 0.05 to 1

Note that the value of the target range used in the simulations is chosen so that the resulting round-trip delay time makes the intermediate frequency (IF) for the target return signal exactly equal to some frequency sample in the power spectrum computed in the simulations to avoid complications in computing the SNR for comparison to the theory due to the target range peak straddling two frequency samples. (This is also why 4 times zero padding works just as well as 8 times zero padding for computing the SNR in the IF power spectrum. Lower amounts of zero padding would also work, but the sidelobes become difficult to discern with the lower amount of upsampling resulting from less zero padding.)

Also note that the value of the average number of additive noise counts per clock time interval, $m_{n\_counts\_avg}$, is twice the value used in the simulations presented in the previous papers [ref 15-17] due to the use of two Gm-APD photon counting detectors in the wavelength tagging version of the dual unipolar bitstream PC-CAML receiver architecture shown in figure 1 (b.). Each Gm-APD has the same value of the average number of additive noise counts per clock time interval as used for the single Gm-APD receiver simulated previously [ref 15-17]. Thus, the total average number of additive noise counts per clock time interval from combining the signals plus noise from each of the two Gm-APDs used in the dual unipolar signal bitstream PC-CAML receiver is twice that for the single Gm-APD used in the single unipolar signal bitstream PC-CAML receiver simulated in the previous work. [ref 15-17]

Figure 2 shows plots of the mean electrical power SNR vs. mean signal counts per clock time interval ($m_{s\_counts\_avg}$) from the simulations and the SNR theory for the dual unipolar chirped sinusoidal signal and bipolar chirped square wave DLLOs with digital I/Q demodulation as a function of $m_{s\_counts\_avg}$ for M=1 and M=1E+06, with $m_{n\_counts\_avg}$=2E-04.

The simulation results and the theory are qualitatively different in that the simulation results for M = 1 and M = 1E+06 do not differ significantly even for higher signal levels as they do for the SNR Theory results. See the earlier discussion of a tentative conjecture to explain this in subsection 2.2. Even so, for the dual unipolar chirped sinusoidal signal, the SNR values for the simulation results for both low and high M are within about ±3 dB of the initial SNR theory values for high M over the range of $m_{s\_counts\_avg}$ plotted.

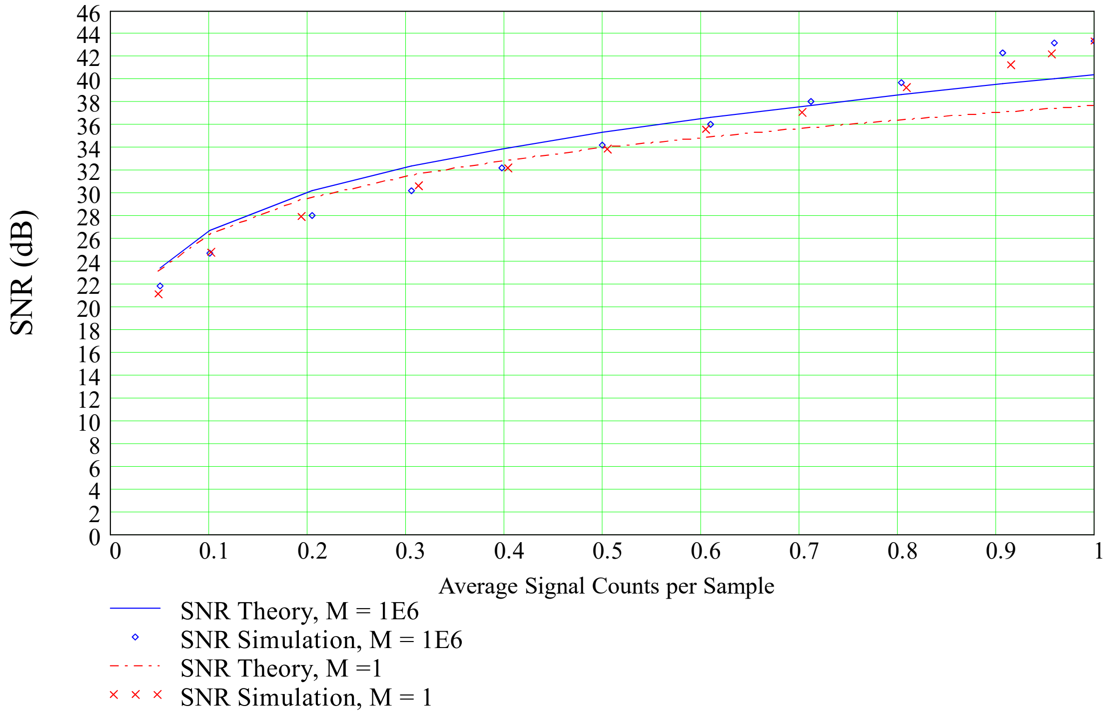

Figure 2. Comparison of SNR results for the Monte Carlo simulations for the dual unipolar chirped sinusoidal signal and bipolar chirped square wave DLLOs with digital I/Q demodulation, and the SNR theory as a function of average signal counts per clock time interval, $m_{s\_counts\_avg}$, with the average number of noise counts per clock time interval, $m_{n\_counts\_avg}$, set equal to 2E-04.

At $m_{s\_counts\_avg}$ above about 0.8, the SNR values for the dual unipolar chirped sinusoidal signal simulation results exceed those of the SNR theory, whereas the SNR values for the unipolar chirped sinusoidal signal simulation results roll over to approach zero as $m_{s\_counts\_avg}$ approaches 1. [ref 15-17]

As explained in section 2.1, the latter behavior is due to the clock time interval samples all being filled with 1's as $m_{s\_counts\_avg}$ approaches 1 for the unipolar chirped sinusoidal signal. This looks like a loss in modulation depth for the sinusoidal signal until at $m_{s\_counts\_avg} = 1$, the modulation depth goes to 0 and the signal looks like a constant level signal with no modulation.

As explained in section 2.1, for the fully modulated dual unipolar chirped sinusoidal signal and for the fully modulated unipolar chirped square wave signal, however, the clock time interval samples where the zero's of the signal waveform are located are never filled by 1's for any signal level, and those clock time interval samples can only have an occasional 1 due to noise at the low noise levels in the simulations and in a well designed PC-CAML. Therefore, as $m_{s\_counts\_avg}$ approaches 1, only the clock time interval samples corresponding to the non-zero levels of waveforms become filled with 1's, and this causes the waveform to approach the uniformly sampled deterministic chirped square wave plus noise waveform as $m_{s\_counts\_avg}$ approaches 1.

Note that a well designed PC-CAML system using transmitter power and/or receiver throughput control to prevent saturation would operate at signal levels below the onset of saturation where the initial SNR theory for large M is at or above the simulation results, i.e, for $m_{s\_counts\_avg}$ values of about 0.6 or less. For these signal levels, these SNR results for the dual unipolar signal and bipolar DLLOs with digital I/Q demodulation are also from about 3 dB to about 6 dB higher than those for the unipolar chirped sinusoidal signal shown in reference 17.

The SNR improvement at the lower signal levels is less than the 6 dB SNR improvement expected for a bipolar signal over that of a unipolar signal because of the higher additive noise due to using two Gm-APDs instead one Gm-APD as explained above. The additive noise is larger relative to the signal shot noise at the lower signal levels so that it has a larger effect on reducing the SNR improvement at lower signal levels.

In addition, since the average quantization noise per clock time interval is proportional to the average signal plus additive noise counts per clock time interval (see equation (4.)), and the signal plus additive noise levels are higher for the dual unipolar signal bitstream PC-CAML than those for the unipolar signal bitstream PC-CAML, then the average quantization noise level per clock time interval is also higher for the dual unipolar signal bitstream PC-CAML than for the unipolar signal bitstream PC-CAML.

On the other hand, if the signal levels are allowed to approach Gm-APD saturation, the fully modulated dual unipolar signal bitstream PC-CAML shows an SNR improvement that is larger than 6 dB at higher signal levels approaching saturation due to its continued increase in SNR with higher signal levels approaching saturation compared to the decreasing SNR with higher signal levels approaching saturation for the unipolar chirped sinusoidal signal bitstream PC-CAML. The unipolar chirped sinusoidal signal bitstream PC-CAML's simulated SNR shown in reference 17 peaks at about 30 dB for an $m_{s\_counts\_avg}$ between 0.6 and 0.7, whereas the dual unipolar signal PC-CAML reaches a maximum simulated SNR of about 43 dB for an $m_{s\_counts\_avg}$ of 1, and is about 37 dB for an $m_{s\_counts\_avg}$ between 0.6 and 0.7.

4. Conclusion

The concept and initial performance modeling and simulation results for the dual unipolar signal with bipolar DLLOs and digital I/Q demodulation technique for the bitstream PC-CAML were presented above. The results of the initial SNR theory and Monte Carlo simulations presented herein indicate that for signal levels below the onset of receiver saturation, the new dual unipolar signal technique for the bitstream PC-CAML improves the electrical power SNR by from about 3 dB to 6 dB compared to that of the unipolar chirped sinusoidal signal with bipolar DLLOs and digital I/Q demodulation [ref 17]. The dual unipolar signal technique provides an improvement in maximum achievable SNR of about 13 dB if the receiver is allowed to saturate. [ref 17]

The bitstream PC-CAML with a dual unipolar signal and bipolar DLLOs with digital I/Q demodulation architecture discussed in this paper adds complexity to the transmitter and receiver compared to the architectures presented in the previous papers. Whether or not this additional complexity is worth the improved SNR will have to be decided as part of system trade studies for particular systems and their applications.

However, the new architecure still retains the key advantages of the previous bitstream PC-CAML architectures [ref 15-17] since it still replaces bulky, power-hungry, and expensive wideband RF analog electronics in the receiver with digital components that can be implemented in inexpensive silicon complementary metal-oxide-semiconductor (CMOS) read-out integrated circuits (ROICs) to make the bitstream PC-CAML with a DLLO more suitable for compact lidar-on-a-chip systems and lidar array receivers than previous standard PC-CAML systems.

5. Suggestions for Future Work

Suggestions for future work include:

1. Develop an SNR theory that includes the effects of quantization noise, aliasing, the harmonics and their mixing products, any signal modulation depth, synchronization errors between the dual unipolar signal channels, and Gm-APD saturation that is applicable to unipolar and dual unipolar chirped sinusoidal and square wave signals for any dead times, matched filter impulse response times, and clock time intervals.
2. Investigate CDMA tagging for the two channels of the dual unipolar signal.
3. Determine if negative binomial plus Poisson (NBPP) distributed random sampling is alias-free for all spectra for any number of count samples accumulated. [ref 15]
4. For bitstream PC-CAML with a DLLO, investigate detection at a harmonic frequency as used for improved range resolution in bitstream radar. [ref 15 and 20]
5. Investigate techniques for suppressing harmonics and sidelobes for application to the bitstream PC-CAML with a DLLO system.
6. Investigate eliminating the high power RF electronics in the bitstream PC-CAML transmitter by using, for example, very low power photonic integrated circuit (PIC) laser sources that can be directly modulated at low voltage and current or followed with low voltage and current PIC waveguide modulators, the modulated output of which is amplified by semiconductor optical amplifiers (SOAs) or optical fiber amplifiers. [ref 22]
7. Perform lab experiments to verify the SNR theory and Monte Carlo simulation results.
8. Build and test breadboard and brassboard bitstream PC-CAML with a DLLO prototypes.

6. Acknowledgments

The author thanks Philip Gatt of Lockheed Martin Coherent Technologies (LMCT) and Barry Stann of the United States Army Research Laboratory (ARL) for their helpful discussions and suggestions. The work reported herein was funded and executed solely by the author.

7. References:

1. Patent US7675610B2, “Photon counting, chirped AM LADAR system and related methods,” Inventors: Brian Redman, William C. Ruff, and Barry L. Stann, Assignee: US Secretary of Army. Available at https://patents.google.com/patent/US7675610B2/en .
2. Brian Redman, William Ruff, and Mark Giza, "Photon counting chirped AM ladar: concept, simulation, and initial experimental results," Proc. SPIE 6214, Laser Radar Technology and Applications XI, 62140P, 19 May 2006.
3. Brian Redman, William Ruff, and Mark Giza, “Photon Counting Chirped AM Ladar: Concept, Simulation, and Experimental Results,” 25th Army Science Conference, AP-14, November, 2006. Available at https://apps.dtic.mil/dtic/tr/fulltext/u2/a481357.pdf

4. B. Redman, W. Ruff, and M. Giza, "Photon Counting Chirped AM Ladar: Concept and Simulation Results," Conference on Lasers and Electro-Optics/Quantum Electronics and Laser Science Conference and Photonic Applications Systems Technologies, Technical Digest, paper PthA4, 2006.

5. Brian C. Redman and Barry L. Stann, “Photon Counting Chirped Amplitude Modulation Ladar,” Army Research Laboratory Technical Report, ARL-TN-305, March, 2008. Available at https://www.arl.army.mil/arlreports/2008/ARL-TN-305.pdf .

6. Zijing Zhang, Long Wu, Yong Zhang, and Yuan Zhao, "Method to improve the signal-to-noise ratio of photon-counting chirped amplitude modulation ladar," Appl. Opt. 52, pp. 274-279, 2013.

7. Zijing Zhang, Yuan Zhao, Yong Zhang, Long Wu, and Jianzhong Su, "Improvement of range accuracy of photon counting chirped AM ladar using phase postprocessing," Appl. Opt. 52, pp. 2447-2453, 2013.

8. Zijing Zhang, Jianlong Zhang, Long Wu, Yong Zhang, Yuan Zhao, and Jianzhong Su, "Photon-counting chirped amplitude modulation lidar using a smart premixing method," Opt. Lett. 38, pp. 4389-4392, 2013.

9. Zhaohui Li, Zeyu Bao, Yafan Shi, Baicheng Feng, E. Wu, Guang Wu, and Heping Zeng, "Photon-Counting Chirped Amplitude Modulation Lidar With 1.5-GHz Gated InGaAs/InP APD," IEEE Photonics Technology Letters, vol. 27, no. 6, pp. 616-619, March 15, 2015.

10. Zijing Zhang, Longzhu Cen, Jiandong Zhang, Kun Ma, Feng Wang, and Yuan Zhao, "Photon counting chirped amplitude modulation lidar using an asymmetric triangular wave modulation," Proc. SPIE 10141, Selected Papers of the Chinese Society for Optical Engineering Conferences held July 2016, 101410V, 7 November 2016.

11. Zijing Zhang, Long Wu, and Yuan Zhao, “Premixing photon-counting chirped amplitude modulation lidar for range and velocity measurement in photon starved scenes,” Optik, Volume 127, Issue 24, pp. 11800-11806, December 2016. Available at this link: https://kundoc.com/pdf-premixing-photon-counting-chirped-amplitude-modulation-lidar-for-range-and-veloc.html (click on the PDF Reader tab to view/download the paper).

12. Yi-Fei Sun, Zi-Jing Zhang, Li-Yuan Zhao, Wei-Min Sun, and Yuan Zhao, “Detection performance improvement of photon counting chirped amplitude modulation lidar with response probability correction,” Chinese Physics B, Volume 27, Number 9, 2018. Available at this link: http://cpb.iphy.ac.cn/article/2018/1953/cpb_27_9_094213.html .

13. Zhou Hui, He Yu-Hao, Lü Chao-Lin, You Li-Xing, Li Zhao-Hui, Wu Guang, Zhang Wei-Jun, Zhang Lu, Liu Xiao-Yu, Yang Xiao-Yan, and Wang Zhen, “Photon-counting chirped amplitude modulation lidar system using superconducting nanowire single-photon detector at 1550-nm wavelength,” Chinese Physics B, 27(1): 018501, 2018. Available at this link: http://cpb.iphy.ac.cn/article/2018/1919/cpb_27_1_018501.html .

14. Zijing Zhang, Long Wu, Yu Zhang, Yuan Zhao, and Xiudong Sun, “Detection performance improvement of chirped amplitude modulation ladar based on Gieger-mode [sic] avalanche photoelectric detector,” Applied Optics, Vol. 50, No. 35, pp. 6522-6525, 10 December 2011.

15. Brian Redman, “Bitstream Photon Counting Chirped AM Lidar with a Digital Logic Local Oscillator,” EngrXiv.org preprint, November, 2019. Available at https://engrxiv.org/bg4m7/ .

16. Brian Redman, “Bipolar Digital Logic Local Oscillator for Bitstream Photon Counting Chirped AM Lidar,” EngrXiv.org preprint, December, 2019. Available at this URL: https://engrxiv.org/7mcbg/ .

17. Brian Redman, “Bitstream Photon Counting Chirped AM Lidar with Digital I/Q Demodulation,” EngrXiv.org preprint, January, 2020. Available at this URL: https://engrxiv.org/drw2m/

18. U.S. Provisional Patent Application Number 62964222, “Bitstream Photon Counting Chirped Amplitude Modulation Lidar with a Dual Unipolar Signal,” Inventor: Brian Carroll Redman, January 22, 2020.

19. Philip Gatt, Steven Johnson, and Terry Nichols, “Geiger-mode avalanche photodiode ladar receiver performance characteristics and detection statistics,” Applied Optics, Vol. 48, No. 17, pp. 3261-3276, 10 June 2009.

20. Øystein Bjørndal, “Single Bit Radar Systems for Digital Integration,” Department of Informatics, University of Oslo (UiO) & Norwegian Defence Research Establishment (FFI), September 2013 – September 2017, Thesis submitted for the degree of Philosophiae Doctor, 2017. Available at https://www.duo.uio.no/handle/10852/59510 .

21. Axel Klein, “Logic Operators on Delta-Sigma Bit-Streams,” Math. Comput. Appl. 2018, 23(1), 4. Available at https://doi.org/10.3390/mca23010004 .

22. Christophe Kopp, Segolene Olivier, and Stephane Bernabe, CEA-LETI, see the discussion of Photonic Integrated Circuit (PIC) laser sources and modulators in the paragraphs after figure 4 at https://www.photonics.com/Articles/Silicon_Photonics_Light_Is_the_Ultimate_Medium/a61635 , EuroPhotonics, Spring 2017.